In vivo imaging of brain androgen receptors in rats

Khayum, M. A.; Doorduin, J.; Farinha Antunes, Ines; Kwizera, Chantal; Zijlma, R.; den Boer, J. A.; Dierckx, R. A. J. O.; de Vries, E. F. J.

Published in:
Nuclear Medicine and Biology

DOI:
10.1016/j.nucmedbio.2015.02.003

Nuclear Medicine and Biology 42 (2015) 561–569

Contents lists available at ScienceDirect

Nuclear Medicine and Biology

journal homepage: www.elsevier.com/locate/nucmedbio

In vivo imaging of brain androgen receptors in rats: a [^{18}F]FDHT PET study

M.A. Khayum [a], J. Doorduin [a], I.F. Antunes [a], C. Kwizera [a], R. Zijlma [a], J.A. den Boer [a,b], R.A.J.O. Dierckx [a], E.F.J. de Vries [a,*]

[a] Department of Nuclear Medicine and Molecular Imaging, University of Groningen, University Medical Center Groningen, Groningen, PO BOX 3100, 9700RB, The Netherlands
[b] PRA-Health Sciences, PO Box 200, 9470 AE Zuidlaren, The Netherlands

ARTICLE INFO

Article history:
Received 7 November 2014
Received in revised form 2 January 2015
Accepted 3 February 2015

Keywords:
16β-[^{18}F]fluoro-5α-dihydrotestosterone ([^{18}F]FDHT)
Androgen receptor
Small animal imaging
Neuroimaging
Positron emission tomography

ABSTRACT

Introduction: Steroid hormones like androgens play an important role in the development and maintenance of several brain functions. Androgens can act through androgen receptors (AR) in the brain. This study aims to demonstrate the feasibility of positron emission tomography (PET) with 16β-[^{18}F]fluoro-5α-dihydrotestosterone ([^{18}F]FDHT) to image AR expression in the brain.
Methods: Male Wistar rats were either orchiectomized to inhibit endogenous androgen production or underwent sham-surgery. Fifteen days after surgery, rats were subjected to a 90-min dynamic [^{18}F]FDHT PET scan with arterial blood sampling. In a subset of orchiectomized rats, 1 mg/kg dihydrotestosterone was co-injected with the tracer in order to saturate the AR. Plasma samples were analyzed for the presence of radioactive metabolites by radio-TLC. Pharmacokinetic modeling was performed to quantify brain kinetics of the tracer. After the PET scan, the animals were terminated for ex-vivo biodistribution.
Results: PET imaging and ex vivo biodistribution studies showed low [^{18}F]FDHT uptake in all brain regions, except pituitary. [^{18}F]FDHT uptake in the surrounding cranial bones was high and increased over time. [^{18}F]FDHT was rapidly metabolized in rats. Metabolism was significantly faster in orchiectomized rats than in sham-orchiectomized rats. Quantitative analysis of PET data indicated substantial spill-over of activity from cranial bones into peripheral brain regions, which prevented further analysis of peripheral brain regions. Logan graphical analysis and kinetic modeling using 1- and 2-tissue compartment models showed reversible and homogenously distributed tracer uptake in central brain regions. [^{18}F]FDHT uptake in the brain could not be blocked by endogenous androgens or administration of dihydrotestosterone.
Conclusion: The results of this study indicate that imaging of AR availability in rat brain with [^{18}F]FDHT PET is not feasible. The low AR expression in the brain, the rapid metabolism of [^{18}F]FDHT in rats and the poor brain penetration of the tracer likely contributed to the poor performance of [^{18}F]FDHT PET in this study.

1. Introduction

Androgens, like testosterone, dihydrotestosterone (DHT) and androstenedione, play a major role in the development and maintenance of sexual characteristics in males. However, androgens are also involved in maintenance of central nervous system functions and in sexual differentiation of the brain in both males and females. In ageing men, the levels of circulating androgens decrease as a result of hypogonadism during a phase called the andropause. An imbalance in the levels of circulating androgens and dysfunction of the hypothalamic-pituitary-gonadal axis are associated with psychiatric problems like mood disorders, psychosis and aggression [1,2]. Partial androgen deficiency may lead to weakness, decreased libido and erectile dysfunction, lower psychological vitality, depressive mood, anxiety, insomnia, difficulty in concentrating and memory impairment. These symptoms overlap with disease characteristics of major depression [3,4]. Testosterone treatment can enhance several aspects of mood and cognition in hypogonadal men [5], it normalizes synaptic neurogenesis, and it reduces depressive symptoms [6]. Still, the role of reduced androgens in psychiatric problems, such as mood disorders, remains largely unknown.

All androgens exert their activity through androgen receptors (AR), which act as transcription factors and alter the expression of androgen-responsive genes. These genes can affect different cellular mechanisms involved in neurogenesis, cell death, cell migration, synapse formation, synapse elimination, and cell differentiation [7]. Despite the role of AR in crucial processes in the healthy and diseased brain, the expression of the receptor in the brain has not been widely studied yet. This is likely due to the lack of validated tools for the non-invasive assessment of AR expression in the living brain. Positron emission tomography (PET) is an imaging technique that can provide information

* Corresponding author at: Department of Nuclear Medicine and Molecular Imaging, University Medical Center Groningen, PO Box 30.001, 9700 RB Groningen, The Netherlands. Tel.: +31 50 3613599; fax: +31 50 3611687.
E-mail address: e.f.j.de.vries@umcg.nl (E.F.J. de Vries).

http://dx.doi.org/10.1016/j.nucmedbio.2015.02.003
0969-8051/

about the expression of receptors in the whole brain in a noninvasive manner, provided that a suitable tracer is available. 16β-[^{18}F]fluoro-5α-dihydrotestosterone ([^{18}F]FDHT) is an ^{18} F-labeled androgen derivative that has been used successfully as a PET tracer for imaging of AR expression in rats, baboons and patients with prostate cancer. However, there are no studies reported yet on the use of [^{18}F]FDHT PET for imaging of AR expression in the brain [8]. The aim of this study was therefore to investigate the feasibility of AR imaging in the rat brain using [^{18}F]FDHT PET. In addition, we investigated whether the [^{18}F]FDHT PET signal is influenced by endogenous or externally administered androgens.

2. Materials and methods

2.1. Animals

Male out-bred Wistar-Unilever rats (13–15 weeks old, 300–400 g) were obtained from Harlan (Horst, The Netherlands). The rats were housed in groups in Macrolon cages with a layer of wood shavings. Animals were housed in a room with constant temperature (21 ± 2 °C), and fixed 12 h light–dark regime. Standard laboratory chow and water were available ad libitum. After arrival, the rats were allowed to acclimatize for at least 7 days. All experiments were approved by the Institutional Animal Care and Use Committee of the University of Groningen, Groningen, the Netherlands (protocol number: DEC5842C).

2.2. Study design

Rats were orchiectomized to reduce the level of circulating androgens that might compete with the PET tracer for the AR binding site and a group of rats underwent sham-orchiectomy and normal circulating androgen levels were thus maintained. Twenty rats were included, but 3 animals could not complete the whole study and therefore were excluded: 1 rat died between surgery and the PET scan and arterial blood sampling failed in 2 rats. One rat (sham-orchiectomized) was excluded from kinetic modeling only, since no reliable time activity curves of the brain could be generated as a result of movement of the animal during the PET scan.

Fifteen days after orchiectomy or sham-surgery, a 90-min dynamic [^{18}F]FDHT PET scan with arterial blood sampling was acquired. Half of the orchiectomized rats were injected with the PET tracer mixed with 1 mg/kg dihydrotestosterone (ORC + DHT; n = 6) as a competitor for binding to the AR in the brain. The remaining orchiectomized (ORC; n = 6) rats received the tracer mixed with vehicle and were used as controls. The sham-orchiectomized animals (Sham ORC; n = 5) received the tracer mixed with vehicle only. After the PET scan, the animals were terminated for ex-vivo biodistribution or analysis of radioactive metabolites in the brain.

2.3. Orchiectomy

Orchiectomy was performed under anesthesia (5% isoflurane in oxygen for induction and 2.5% for maintenance). Rats were placed in a supine position exposing the testes. A surgical incision of about 1 cm was made on midline of the scrotum, and the skin of scrotum was pulled towards each lateral side to expose the testes in the tunica vaginalis. A small orifice was made by pulling the tunica vaginalis, and the testes were exteriorized along with epididymis and vas deferens. The blood vessels supplying the testes (arteries and veins) from the top and the bottom were ligated and the testes along with the epididymis and the vas deferens were removed. Biodegradable sutures were made in the tunica vaginalis and the skin of midline scrotum. Immediately after surgery rats received a subcutaneous injection of finadyne (2.5 mg/kg Flunixin, Schering-Plough N.V/S.A., Belgium) for pain relief, and administration of pain medication was repeated 24 h after surgery. Rats were allowed to recover for 14 days, before they were subjected to PET imaging. In the sham-orchiectomized group, the same surgical procedure was performed, but without ligation of the blood vessels and removal of the testes.

2.4. [^{18}F]FDHT synthesis

[^{18}F]FDHT was produced by modification of the procedure described by Liu et al. 1992 [9] (Fig. 1). Cyclotron-produced [^{18}F]fluoride was trapped on a QMA anion exchange cartridge (Waters). The cartridge was eluted with a solution consisting of 0.2 ml of a 5 mg/ml aqueous potassium carbonate solution and 0.7 ml of a 15 mg kryptofix[2.2.2] solution in acetonitrile. The eluate containing the K[^{18}F]-kryptofix complex was dried by azeotropic distillation with dry acetonitrile (3×0.5 ml). After drying, a solution of 2 mg of the triflate precursor (Fig. 1) in 0.5 ml of dry acetonitrile was added. The reaction mixture was heated at 55 °C for 5 min and subsequently the solvent was evaporated at 70 °C for 10 minutes. A solution of 5 mg of sodium borohydride in 1 ml of ethanol was added at 30 °C. After 5 min, 0.5 ml of 1 M HCl was slowly added and the product was hydrolyzed for 15 min at 85 °C. The mixture was then passed through an Alumina N cartridge and an Acrodisc 1.2 μm filter in order to remove the free [^{18}F]fluoride and precipitated particles. Via the cartridge and filter, 300 mg sodium acetate trihydrate in 0.8 ml of water was added to the eluate for neutralization. The mixture was purified by HPLC (SymmetryPrep C18 column (7 μ, 7.8×300 mm), eluent: 42% acetonitrile in water, flow 4 ml/min). [^{18}F]FDHT, with a retention time of approximately 15 min, was collected and diluted into 50 ml of water. The solution was then applied to an Oasis HLB 1 cc (30 mg) cartridge and the cartridge was washed with 3×5 ml of water. The final product was eluted with 1 ml of ethanol and 10 ml of 0.9% NaCl. The product was sterilized by filtration over a 0.22 μm LG filter and collected in a 25 ml sterile vial. Quality control was performed by Ultra-high performance chromatography (UPLC) (column: Acquitiy UPLC BEH C18 (1.7 μ, 2.1×50 mm, eluent: 30% acetonitrile in water). The identity of [^{18}F]FDHT was verified by co-elution with an authentic reference sample. For the final formulation for in vivo experiments, the tracer was diluted with saline and reconstituted with 30% beta-cyclodextrin.

2.5. PET acquisition

Rats were anesthetized with isoflurane mixed with medical air (5% for induction and 2.5% for maintenance) and a catheter (0.8 mm o.d.; 0.4 mm i.d.) was inserted into the femoral vein for the injection of [^{18}F]FDHT and another catheter was inserted into the femoral artery for blood sampling. After cannulation, the rats were positioned into the PET scanner (Focus 220, Siemens Medical Solutions, USA, Inc.) in a transaxial position with their heads in the center of the field of view. A transmission scan of 515 seconds with a ^{57}Co point source was obtained for the correction of attenuation and scatter by tissue. After the transmission scan was completed, 23 ± 12 MBq [^{18}F]FDHT (specific activity 89 ± 56 GBq/nmol), mixed with either 30% beta-cyclodextrin or with 1 mg/kg DHT (Sigma-Aldrich, USA) in 30% beta-cyclodextrin, was injected over a period of 1 min into the femoral vein cannula using an infusion pump. Simultaneously with the injection of [^{18}F]FDHT, an emission scan of 90 min was started. During the PET acquisition 16 blood samples were collected to construct the plasma input function and to determine the percentage of plasma metabolites.

2.6. Arterial blood sampling and metabolite analysis

Blood samples of approximately 100 μl were collected at approximately 10, 20, 30, 40, 50, 60, 90, 120, 180, 300, 450, 600, 900, 1800, 3600, and 5400 seconds after [^{18}F]FDHT injection. After collection of each blood sample, 0.1 ml of heparinized saline was injected to prevent large changes in blood pressure. From the collected blood, 25 μl of blood was collected separately to generate a whole blood activity curve. The

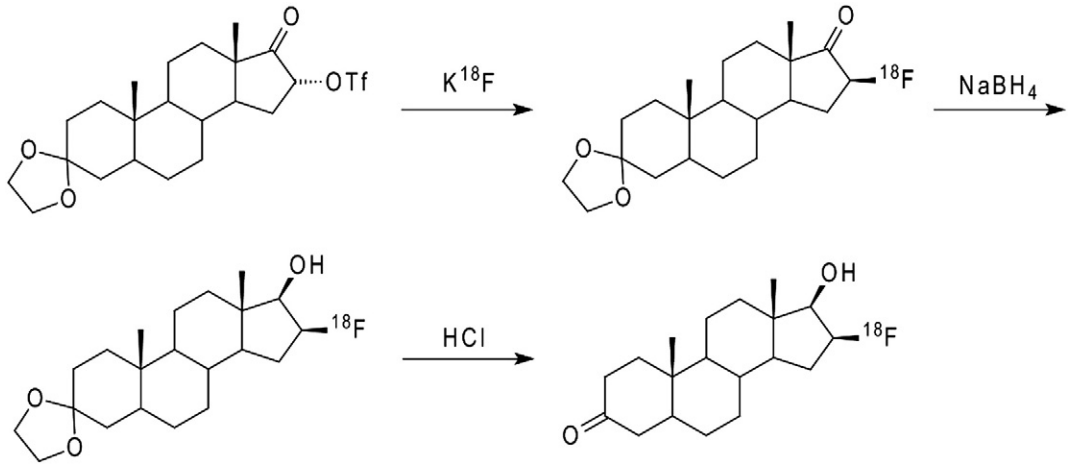

Fig. 1. Radiolabeling of [^{18}F]FDHT.

rest of the blood was centrifuged at 13,000 rpm for 5 min. The radioactivity in 25 μl of whole blood and in 25 μl of plasma was measured using a gamma counter (LKB Wallace, Turku, Finland). After the radioactivity measurement, 50 μl of acetonitrile was added to the plasma samples in order to precipitate the proteins. Hereafter, the mixture was vortexed and centrifuged at 13,000 rpm for 5 min. Radioactivity in the supernatant and the pellet was measured to calculate recovery of activity (Recovery of activity = [Activity(supernatant)/(Activity(supernatant) + Activity(pellet)] * 100%). An aliquot of 5 μl of the supernatant was applied on a silica gel TLC strip. The TLC strip was dried and run with an eluting medium consisting of n-hexane and ethyl acetate (3:2). After elution, the TLC strip was placed on a phosphor storage screen for overnight exposure. The screen was read out with a Cyclone reader and analyzed with OptiQuant software (OptiQuant version 03.00, Packard Instrument Company) to calculate the percentages of intact parent compound and metabolites. Metabolite analysis failed in 1 orchiectomized rat (without DHT treatment) due to technical reasons; for this animal, a population based metabolite curve was generated from the average metabolite curves of the other orchiectomized rats (without DHT treatment).

2.7. PET image reconstruction and analysis

PET data were normalized and corrected for attenuation, scatter, random coincidences and decay. The list-mode data of the emission scans was separated into 23-frame sinograms (6×10, 4×30, 2×60, 1×120, 1×180, 4×300, 3×600 and 2×900 sec), which were iteratively reconstructed (OSEM2D, 4 iterations, 16 subsets). PET image analysis was performed using Inveon 4.0 software (Siemens Medical Solutions, USA, Inc). The PET scan was manually co-registered with a T2 MRI template. Regions of interest (ROI) were drawn around the amygdala, bed nucleus of stria terminalis (BNST), brainstem, cerebellum, frontal cortex, hippocampus, hypothalamus, midbrain, occipital/temporal/parietal cortex (OTP Cortex), prefrontal cortex, pituitary gland, striatum, thalamus, preoptic area, whole brain, frontal bone, and interparietal bone on the MRI template and transferred to the co-registered PET scans. Time-activity curves were generated for each region of interest. In addition, the activity in the ROI during the last 15 min of the scan was measured (75–90 min) and converted into standardized uptake values (SUV) by normalization for body weight and injected tracer dose. The SUV was defined as: [tissue activity concentration (Bq/cm^3)]/[injected dose (Bq)/body weight (g)]. It was assumed that 1 cm^3 of brain tissue equals 1 g.

Kinetic modeling (compartment modeling and graphical analysis) was used to quantify the brain uptake of [^{18}F]FDHT, using whole blood activity and metabolite-corrected plasma activity as the input functions. For Logan graphical analysis a delay time (T*) of 10 min was applied, whereas a 20 min delay time was used for Patlak analysis. Both the one-tissue compartment model (1TCM) and the two-tissue reversible compartment model (2TRCM) were evaluated, using a fixed blood volume of 3.6%. Both compartment models were used to calculate the volume of distribution (V_T):

$$1\text{TCRM}: V_T = \frac{K_1}{k_2}$$

$$2\text{TCRM}: V_T = \left(\frac{K_1}{k_2}\right) * \left(1 + \frac{k_3}{k_4}\right)$$

The 2TCRM was also used to determine the non-displaceable binding potential (BP_{ND}):

$$BP_{ND} = \frac{k_3}{k_4}$$

2.8. Ex vivo biodistribution

After the 90-min PET scan, rats were sacrificed by extirpation of the heart while under deep anesthesia. The brain and major peripheral tissues were isolated. One hemisphere of the brain was dissected into specific brain regions; the other hemisphere was used for metabolite analysis. Blood was centrifuged (6000×*g* for 5 min) to collect a plasma sample. The tissue and plasma samples were weighed and analyzed for the amount of radioactivity with a gamma counter (LKB-Wallac, Turku, Finland). Tracer uptake was expressed as SUV.

2.9. Brain metabolite analysis

Ninety min after tracer injection, the remaining brain hemisphere was weighed and cut into small pieces. Two volumes of acetonitrile were added and the tissue was homogenized for 2 min. The homogenate was centrifuged at 13,000 rpm for 5 min to remove the particulate cell debris. A sample of the supernatant was collected and analyzed for the presence of radiolabeled metabolites by TLC, as describe above for the analysis of plasma samples.

2.10. Statistical analysis

All data are expressed as mean ± standard error of the mean (SEM). Statistical analysis was performed using IBM SPSS statistics 22. Data were analyzed by one-way ANOVA with groups as factor and brain

regions as independent variables. Time-activity curves were analyzed separately for the distribution phase (0–3 min) and the elimination phase (3–90 min) using a repeated measures ANOVA, with group as the between-subject factor and time as the within-subject factor. ANOVA was followed by a Tukey post-hoc test to correct for multiple comparisons. Significance was reached when the probability (p-value) was <0.05.

3. Results

3.1. [^{18}F[FDHT synthesis

The synthesis of [^{18}F]FDHT was based on the method described by Liu et al., 1992 [9]. In our hands, the published method was not readily applicable for automation, because of the use of low temperatures and moisture-sensitive reagents. Therefore, the labeling procedure was adjusted to allow fully automated production using a disposable cassette-based synthesis module. [^{18}F]FDHT was reliably synthesized, although with a low radiochemical yield of 4.3 ± 1.6%. The product radiochemical purity of 96 ± 3% and a specific activity of 130 ± 30 MBq/nmol. The main impurity – if present – was the 16α-isomer of [^{18}F]FDHT.

3.2. Ex-vivo biodistribution

The results of the ex-vivo brain distribution of [^{18}F]FDHT at 90 min after tracer injection are presented in Table 1. In all groups, [^{18}F]FDHT uptake was highest in pituitary, whereas very low uptake was observed in all other brain regions. Tracer uptake in sham-orchiectomized rats was about 2-fold higher than in the other groups. However, statistical analysis by one-way ANOVA followed by a Tukey posthoc test could not reveal any significant differences in tracer uptake between groups for any of the brain regions. Ex-vivo biodistribution in peripheral organs showed highest tracer uptake (SUV > 1) in excretory organs (kidney, bladder, liver, stomach, duodenum, small intestine), prostate and bone in all groups. However, statistical analysis did not reveal any significant differences in tracer uptake between groups either.

3.3. PET imaging

A representative [^{18}F]FDHT PET image of the brain of an orchiectomized rat is presented in Fig. 2A. Rats of all groups showed low uptake of activity in the brain and high uptake in the surrounding cranial bones. The average time-activity curves (TACs) of the whole brain and interparietal bone are presented in Fig. 2B and C. The [^{18}F]FDHT uptake in the brain peaked around 1.5 min, followed by a rapid washout. [^{18}F]FDHT uptake in the whole brain was not significantly different between groups at any time point (e.g. SUV(75–90 min): 0.16 ± 0.03, 0.26 ± 0.06 and 0.37 ± 0.09 for orchiectomized rats, orchiectomized rats treated with DHT and sham-orchiectomized rats, respectively ($p = 0.09$)). In contrast, statistical analysis of the tracer uptake in the cranial bones revealed a significant group effect in the elimination phase (3–90 min; $F(2,14) = 6.2$, $p < 0.05$), but not in the distribution phase (0–3 min). Tukey post-hoc analysis showed that tracer uptake in the cranial bones was significantly higher in sham-orchiectomized rats than in orchiectomized animals.

Table 1
Ex vivo brain distribution of [^{18}F]FDHT 90 min post injection in orchietomized rats (ORC, n = 6), orchiectomized rats co-injected with 1 mg/kg dihydrotestosterone (ORC + DHT, n = 6) and sham-orchietomized rats (Sham ORC, n = 5). Results are expressed as standardized uptake values (mean ± SEM). Data were analyzed by one-way ANOVA followed by a Tukey post hoc test. No significant differences ($p < 0.05$) between groups were observed. OTP cortex: Occipital, temporal, parietal cortex.

Brain region	ORC	ORC + DHT	Sham ORC
Amygdala	0.019 ± 0.005	0.057 ± 0.011	0.102 ± 0.050
Bulbus olfactorius	0.048 ± 0.014	0.068 ± 0.012	0.072 ± 0.010
Cerebellum	0.040 ± 0.010	0.054 ± 0.008	0.149 ± 0.085
Cingulate Cortex	0.022 ± 0.005	0.052 ± 0.010	0.103 ± 0.047
Entorhinal Cortex	0.037 ± 0.014	0.087 ± 0.031	0.107 ± 0.038
Frontal Cortex	0.034 ± 0.014	0.041 ± 0.007	0.094 ± 0.043
Hippocampus	0.036 ± 0.016	0.043 ± 0.007	0.100 ± 0.042
Hypothalamus	0.049 ± 0.016	0.088 ± 0.031	0.138 ± 0.042
Medulla	0.048 ± 0.016	0.057 ± 0.008	0.135 ± 0.067
OTP Cortex	0.032 ± 0.010	0.040 ± 0.006	0.104 ± 0.048
Pituitary	0.241 ± 0.064	0.241 ± 0.052	0.552 ± 0.166
Pons	0.044 ± 0.012	0.057 ± 0.011	0.117 ± 0.041
Striatum	0.034 ± 0.015	0.058 ± 0.017	0.098 ± 0.047
Thalamus	0.035 ± 0.013	0.050 ± 0.012	0.131 ± 0.064

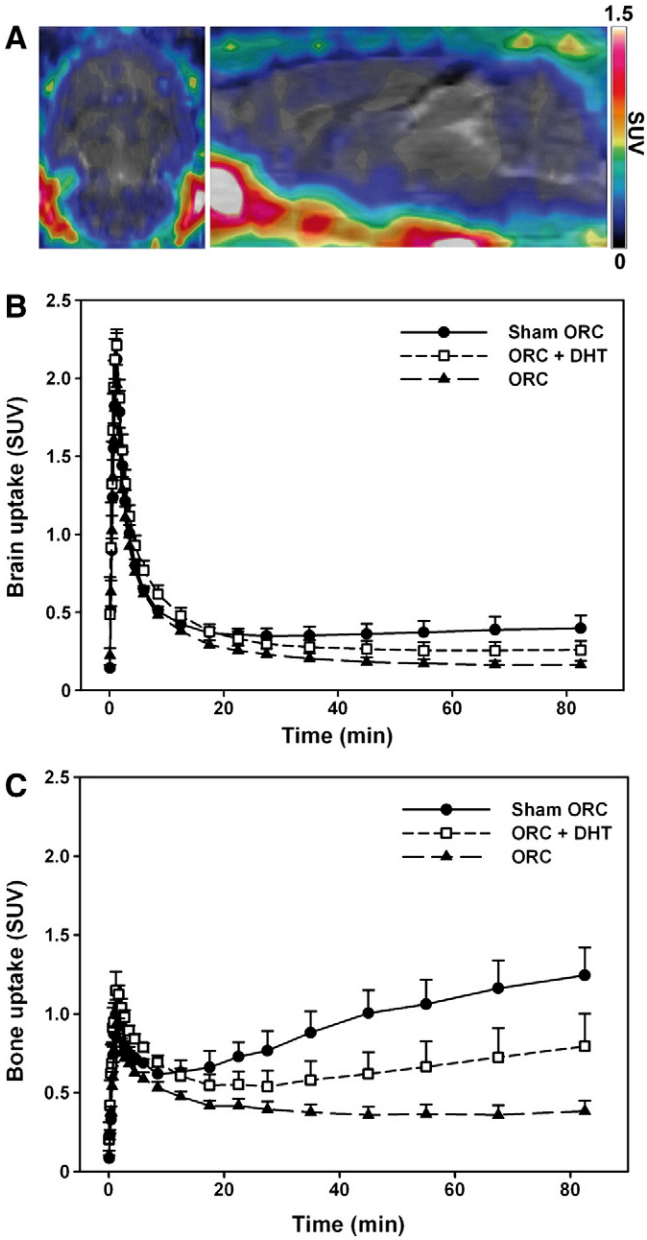

Fig. 2. (A) Representative coronal (left) and sagittal (right) [^{18}F]FDHT PET images of a rat brain. Images consist of the summed data from 50–90 min after tracer injection in a ORC rat. PET images are co-registered with an MRI template for anatomical reference. Time activity curves of [^{18}F]FDHT (standardized uptake value; mean ± SEM) in the whole brain (B) and interparietal bone (C) in orchiectomized rats (ORC, n = 6), orchiectomized rats co-injected with 1 mg/kg dihydrotestosterone (ORC + DHT, n = 6) and sham-orchietomized rats (Sham ORC, n = 5). No significant differences were observed in the time-activity curves in the whole brain. In contrast, [^{18}F]FDHT uptake in cranial bone was significantly higher in the distribution phase (3–90 min) in sham-orchiectomized rats than in orchiectomized rats ($p < 0.05$).

When investigating individual brain regions at 75–90 min post injection, PET imaging showed higher tracer uptake in brain regions located close to cranial bones such as cerebellum, frontal cortex, prefrontal cortex, and pituitary, than in centrally located brain regions (Table 2). ANOVA followed by a posthoc Tukey test showed increased uptake in the brain stem of sham-orchiectomized rats, as compared to both orchiectomized groups ($p < 0.05$). This difference between groups is likely due to spill-over effects from the surrounding cranial bones. To avoid interference of spill-over effects, centrally located brain regions were analyzed separately. After exclusion of brain regions located close to cranial bones, still none of the centrally located brain regions showed any significant differences in tracer uptake between groups.

3.4. Plasma activity and metabolism

[^{18}F]FDHT plasma clearance could be described well with a bi-exponential function in all groups, with a short half-life in the distribution phase and a long half-life in the excretion phase (1.7 ± 0.3 and 12 ± 4 min; 3.9 ± 1.9 and 8 ± 4 min; 19 ± 10 and 3.4 ± 0.2 min for orchiectomized rats, DHT-treated orchiectomized rats and sham-orchiectomized rats, respectively). These differences in half-life between groups were not statistically significant.

[^{18}F]FDHT was rapidly metabolized in all groups of rats (Fig. 3A). Statistical analysis (repeated measures ANOVA) revealed significant differences in the percentage of plasma metabolites between groups ($F(2,13) = 5.5$, $p < 0.05$) in the elimination phase (3–90 min p.i.), but not in the distribution phase (0–2 min p.i.). Tukey post-hoc analysis showed a statistically significant lower percentage of metabolites in plasma during the elimination phase in sham-orchiectomized rats than in DHT-treated orchiectomized rats ($p < 0.05$), whereas the difference between sham-orchiectomized rats and orchiectomized rats was approaching significance ($p = 0.065$). In the sham-orchiectomized rats, 50% of the radioactivity in plasma still consisted of intact tracer at about 15 min after tracer injection, whereas 50% of metabolism of the tracer was already observed within 5 min in both groups of orchiectomized rats.

The metabolite-corrected TACs of plasma are displayed in Fig. 3B. In line with the differences in [^{18}F]FDHT metabolism between groups, also a statistically significant group effect ($F(2,13) = 5.4$, $p < 0.05$) was observed in elimination phase of the metabolite-corrected plasma TACs (3–90 min p.i.), with a statistically significant lower metabolite-corrected plasma activity in the sham-orchiectomized group than in both orchiectomized groups (Tukey posthoc test, $p < 0.05$). The distribution phase (0–2 min p.i.) of the metabolite-corrected plasma curve was not statistically significantly different between groups.

Analysis of [^{18}F]FDHT metabolites in the brain was not successful, because the signals of the intact tracer and its metabolites were below the limit of quantification as a result of the low brain uptake of the tracer.

Table 2
[^{18}F]FDHT uptake 75–90 min post injection in various brain regions of orchietomized rats (ORC, n = 6), orchiectomized rats co-injected with 1 mg/kg dihydrotestosterone (ORC + DHT, n = 7) and sham-orchietomized orchiectomized (Sham ORC, n = 6) rats, as determined by PET. Data are expressed as standardized uptake values (mean ± SEM). Data were analyzed by one-way ANOVA followed by a Tukey post hoc test. Significant differences as compared to the orchiectomized group are indicated with an asterisk: *$p < 0.05$. BNST: bed nucleus of stria terminalis, OTP cortex: Occipital, temporal, parietal cortex.

Brain region	ORC	ORC + DHT	Sham ORC
Brain regions located centrally in the brain			
Amygdala	0.10 ± 0.02	0.18 ± 0.03	0.27 ± 0.08
BNST	0.07 ± 0.02	0.09 ± 0.02	0.15 ± 0.03
Hippocampus	0.09 ± 0.02	0.13 ± 0.03	0.17 ± 0.03
Hypothalamus	0.09 ± 0.02	0.13 ± 0.03	0.26 ± 0.03
Midbrain	0.10 ± 0.02	0.13 ± 0.04	0.16 ± 0.02
Striatum	0.08 ± 0.02	0.11 ± 0.02	0.14 ± 0.03
Thalamus	0.05 ± 0.01	0.10 ± 0.02	0.11 ± 0.03
Preoptic Area	0.13 ± 0.03	0.21 ± 0.06	0.29 ± 0.06
Brain regions close to the cranial bones			
Brainstem	0.10 ± 0.02	0.19 ± 0.04	0.28 ± 0.06*
Cerebellum	0.18 ± 0.03	0.30 ± 0.07	0.44 ± 0.12
Frontal Cortex	0.20 ± 0.04	0.27 ± 0.06	0.44 ± 0.12
OTP Cortex	0.18 ± 0.03	0.26 ± 0.06	0.40 ± 0.11
Prefrontal Cortex	0.23 ± 0.05	0.31 ± 0.07	0.46 ± 0.12
Pitutary	0.21 ± 0.04	0.37 ± 0.10	0.57 ± 0.17

3.5. Graphical analysis

Graphical analysis of tracer kinetics in the brain was performed by Patlak and Logan analysis using the metabolite-corrected plasma curves as input function. Logan graphical analysis showed a good fit (T^* 10 min, r^2 0.96 ± 0.00) for all centrally located brain regions in all groups, suggesting that [^{18}F]FDHT displays reversible kinetics in these regions. In contrast, tracer kinetics in brain regions close to the cranial bones, like prefrontal cortex, brainstem, cerebellum, pituitary, and frontal cortex could be fitted better by Patlak (T^* 20 min, r^2 0.96 ± 0.01) than by Logan graphical analysis. The tracer kinetics in cranial bones were also better described by Patlak than Logan graphical analysis. The irreversible binding in cranial bones suggests accumulation of free [^{18}F]fluoride as a result of defluorination of the tracer. Fig. 4 shows representative examples of Logan and Patlak plots of a brain region located close to cranial bone (occipital/parietal/temporal cortex; OTP Cortex), a centrally located brain region (bed nucleus of stria terminalis; BNST) and the interparietal bone. These results suggest that PET imaging of [^{18}F]FDHT uptake in brain regions in the vicinity of the cranial bones is substantially affected by spill-over effects from the cranial bones into the brain. Sham-orchiectomized rats were most affected by spill-over, since bone uptake is higher in this group of animals than in both orchiectomized groups. To avoid spill-over effects, the brain regions close to the cranial bones were excluded from further analysis. Logan graphical analysis was used to calculate the V_T in central brain regions (Table 3). In all central brain regions, V_T was highest in DHT-treated orchiectomized rats, although the differences between groups were not statistically significant. The difference in V_T in midbrain between sham-orchiectomized rats (0.56 ± 0.07) and DHT-treated orchiectomized rats (1.09 ± 0.17) approached significance (one-way ANOVA, Tukey posthoc test, $p = 0.054$).

3.6. Compartment modeling

Compartment modeling with the 1TCM and 2TRCM was used to quantify the tracer kinetics in the central brain regions (Table 3). Kinetic modeling with the 1TCM model provide V_T values that were approximately 2-fold lower than those obtained by Logan graphical analysis. The V_T determined by the 1TCM did not show any statistically significant differences in V_T between groups.

Application of the 2TRCM resulted in V_T values that were generally higher and showed more variability than V_T calculated by the 1TCM. The V_T determined with the 2TRCM was not significantly different between groups for any of the central brain regions. The 2TRCM was also used to calculate the non-displaceable binding potential (BP_{ND}) for the central brain regions. However, no significant differences in PB_{ND} between groups were observed either.

4. Discussion

[^{18}F]FDHT is a PET tracer that was developed for imaging of AR expression in prostate cancer and the tracer has already been applied for this purpose in several clinical studies [10,11]. So far, [^{18}F]FDHT has not been investigated as a probe for imaging of AR in the brain. In this study, we therefore aimed to establish the feasibility of in vivo quantification of AR availability in the rat brain by [^{18}F]FDHT PET.

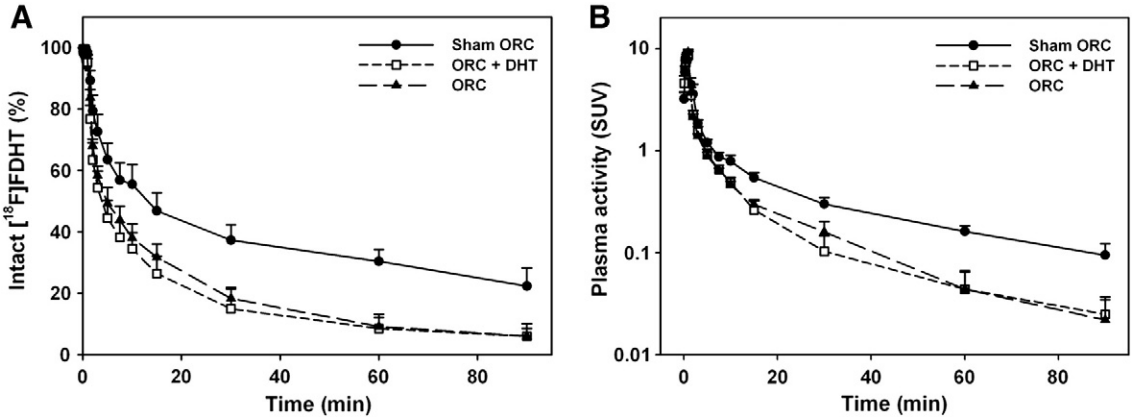

Fig. 3. (A) Percentage of intact [^{18}F]FDHT in plasma and (B) metabolite-corrected plasma curves of [^{18}F]FDHT in orchiectomized rats (ORC, n = 5), orchiectomized rats co-injected with 1 mg/kg DHT (ORC + DHT, n = 6) and sham-orchietomized rats (Sham ORC, n = 5) (mean ± SEM). Sham-orchiectomized rats showed a significantly higher percentage of intact tracer and metabolite-corrected plasma curve in the elimination phase of the time-activity curve (3–90 min, $p < 0.05$).

Our PET imaging and ex vivo biodistribution studies showed that [^{18}F]FDHT uptake in the rat brain was low. The poor brain uptake of [^{18}F]FDHT may be explained by compromised penetration of the tracer across the blood–brain barrier. In theory, [^{18}F]FDHT should be sufficiently lipophilic to passively diffuse into the brain. However, DHT is a known substrate of P-glycoprotein [12]. P-glycoprotein is an efflux transporter in the blood–brain barrier that can extrude a wide variety of lipophilic compounds out of the brain. Because of the structural similarities of [^{18}F]FDHT and DHT, it is conceivable that the PET tracer is also a P-glycoprotein substrate and consequently may not be able to cross the blood–brain barrier. This hypothesis is in line with the observation that [^{18}F]FDHT uptake was substantially higher in pituitary, which is not protected by the blood–brain barrier [13], than in any other brain region. On the other hand, the TACs of [^{18}F]FDHT (Fig. 2B) show a high peak uptake in the brain within 2 minutes after tracer injection (SUV > 2), suggesting that tracer delivery to the brain is not impaired. Moreover, the TAC of [^{18}F]FDHT closely resembles the published TAC of ^{3}H-testosterone [14], which can readily cross the blood–brain barrier. Also the influx constant K1 of FDHT (ca. 0.5 ml/g/min) calculated by compartmental modeling does not suggest any impaired tracer delivery to the brain. Moreover, the K1 value of pituitary was in the same range as the influx constant calculated for the centrally located brain regions. Thus, impaired blood–brain barrier permeability does not seem to be the major contributor to the poor brain uptake of [^{18}F]FDHT in the brain.

Another cause for the low brain uptake of [^{18}F]FDHT could be the fast metabolism of the tracer. This study showed that [^{18}F]FDHT is indeed rapidly [15] metabolized in rats. In human, DHT is mainly bound to sex hormone binding globulin (SHBG) and to lesser extent to albumin, which protect the steroid from degradation. A potential cause for the fast in-vivo degradation of [^{18}F]FDHT observed in this study could be the absence of SHBG in rats [16]. Radio-TLC of rat plasma showed that all metabolites of [^{18}F]FDHT were more polar than the parent compound. Although we did not identify the nature of these metabolites, it is expected that the main metabolites consist of glucuronides or sulfates of the tracer, which are unlikely to penetrate the blood–brain barrier. Beattie and coworkers have isolated the radiolabelled metabolites of [^{18}F]FDHT from human serum and exposed them in-vitro to CWR22 cells [15]. They showed that the radiolabeled metabolites of [^{18}F]FDHT could not enter the cells or bind to the cell membrane. If the [^{18}F]FDHT metabolites cannot cross the cell membrane, it seem plausible that they also cannot penetate the blood–brain barrier. A limitation of our study was that we were not able to measure the percentage of [^{18}F]FDHT metabolites in the brain, because the intensity of the signals

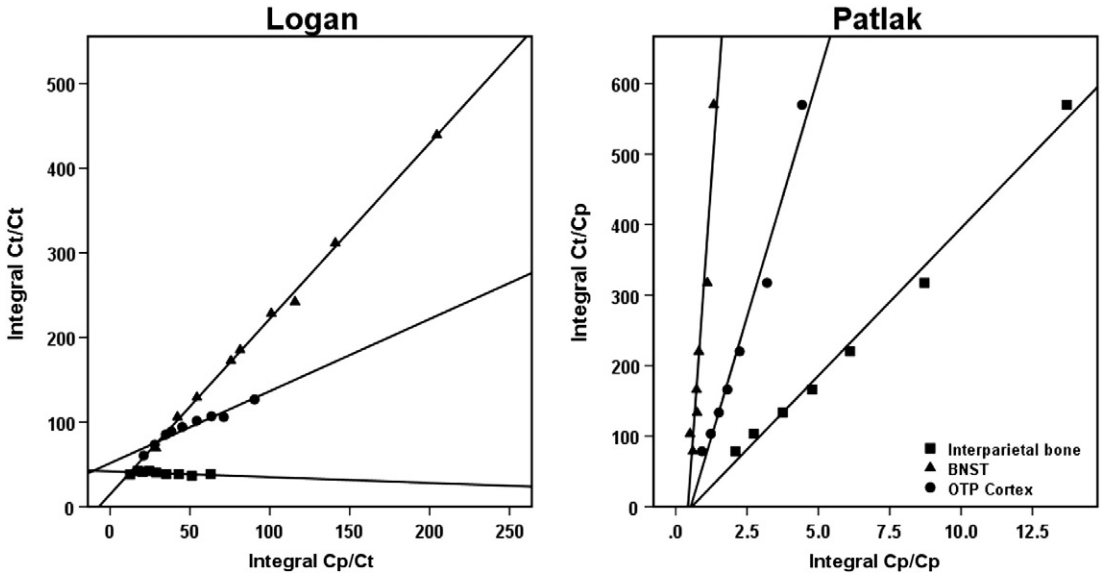

Fig. 4. Average Logan (left) and Patlak plots (right) of interparietal bone, bed nucleus of stria terminalis (BDNS) and occipital/temporal/parietal cortices (OTP Cortex) of Sham ORC rats (n = 4).

Table 3
Results of kinetic modeling of [^{18}F]FDHT in orchietomized rats (ORC, n = 6), orchiectomized rats co-injected with 1 mg/kg dihydrotestosterone (ORC + DHT, n = 6) and sham-orchietomized orchiectomized rats (Sham ORC, n = 4), using Logan graphical analysis and kinetic modeling with a one-tissue compartment model (1TCM) or a two-tissue reversible compartment model (2TRCM). Blood volume was a fixed at 3.6%. Statistical analysis was performed by one-way ANOVA followed by a Tukey post hoc test. Data are presented as mean ± SEM. No significant differences ($p < 0.05$) between groups were observed. BNST: bed nucleus of stria terminalis.

Brain region	VT (Logan)			VT (1TCM)			VT (2TRCM)			BP (2TRCM)		
	ORC	ORC + DHT	Sham ORC	ORC	ORC + DHT	Sham ORC	ORC	ORC + DHT	Sham ORC	ORC	ORC + DHT	Sham ORC
Amygdala	0.80 ± 0.15	1.20 ± 0.22	0.70 ± 0.20	0.43 ± 0.05	0.43 ± 0.05	0.36 ± 0.06	0.59 ± 0.08	1.10 ± 0.27	0.97 ± 0.34	1.6 ± 0.5	2.2 ± 0.5	1.8 ± 0.5
BNST	0.67 ± 0.11	0.93 ± 0.15	0.52 ± 0.09	0.44 ± 0.04	0.46 ± 0.06	0.31 ± 0.04	0.59 ± 0.06	0.98 ± 0.27	0.48 ± 0.07	2.2 ± 0.9	2.0 ± 0.4	1.0 ± 0.1
Hippocampus	0.70 ± 0.11	1.00 ± 0.16	0.57 ± 0.07	0.40 ± 0.04	0.42 ± 0.05	0.32 ± 0.05	0.55 ± 0.07	0.79 ± 0.11	0.45 ± 0.05	3.5 ± 1.9	1.9 ± 0.3	1.6 ± 0.7
Hypothalamus	0.76 ± 0.11	1.10 ± 0.19	0.71 ± 0.20	0.42 ± 0.04	0.42 ± 0.04	0.35 ± 0.05	0.58 ± 0.04	0.85 ± 0.17	0.65 ± 0.25	1.9 ± 0.5	2.0 ± 0.3	1.4 ± 0.3
Midbrain	0.77 ± 0.11	1.09 ± 0.17	0.56 ± 0.07	0.45 ± 0.05	0.47 ± 0.05	0.37 ± 0.06	0.58 ± 0.08	0.70 ± 0.07	0.48 ± 0.06	1.8 ± 0.9	1.9 ± 0.3	0.9 ± 0.3
Preoptic Area	0.82 ± 0.15	1.14 ± 0.20	0.73 ± 0.14	0.42 ± 0.07	0.41 ± 0.06	0.31 ± 0.07	0.72 ± 0.15	1.50 ± 0.57	1.41 ± 0.61	2.2 ± 0.5	3.7 ± 1.2	4.6 ± 2.4
Striatum	0.72 ± 0.12	1.01 ± 0.14	0.55 ± 0.09	0.42 ± 0.05	0.46 ± 0.05	0.35 ± 0.06	0.55 ± 0.04	0.76 ± 0.10	0.49 ± 0.09	2.2 ± 0.6	2.5 ± 0.5	1.4 ± 0.6
Thalamus	0.68 ± 0.10	0.93 ± 0.13	0.53 ± 0.10	0.44 ± 0.05	0.46 ± 0.05	0.35 ± 0.06	0.56 ± 0.06	0.65 ± 0.07	0.47 ± 0.07	1.7 ± 0.3	2.2 ± 0.4	0.9 ± 0.1

for both the intact tracer and the metabolites was below the limit of quantification. Taken together, poor availability of the intact tracer in plasma due to rapid metabolism seems to contribute to the low brain uptake of [^{18}F]FDHT. This hypothesis is supported by the observation that the sham-orchiectomized group revealed significantly slower metabolism of [^{18}F]FDHT and a trend towards higher brain uptake (SUV) than both the orchiectomized groups. It remains unclear why sham-orchiectomized rats show slower tracer metabolism than orchiectomized animals. Possibly, competition between endogenous androgens and the PET tracer for the metabolising enzymes, or up-regulation of metabolising enzymes in orchiectomized rats could play a role. Studies in pig have shown that castration causes an increase in the expression of hydroxysteroid hydrogenases in the liver [17,18]. These enzymes play an important role in the metabolism of DHT, as they catalyse the conversion of DHT into 5α-androstan-3α/β,17β-diol, which is further metabolised into the corresponding glucuronide by uridine diphosphate glucuronyl transferase [19].

In addition to the metabolites found in plasma, [^{18}F]FDHT is likely also degraded by defluorination. The accumulation of free [^{18}F]fluoride could account for the increasing uptake of radioactivity in the cranial bones over time. Accumulation of activity in the cranial bones is significantly higher in sham-orchiectomized rats than in both orchiectomized groups. Orchiectomy can cause an increase in the activity of the metabolic liver enzymes, resulting in increased tracer metabolism in the orchiectomized groups. In sham-orchiectomized animals, more intact tracer remains available that can release more free fluoride, which subsequently can accumulate in the bone.

Extensive defluorination of [^{18}F]FDHT has previously already been observed in rats [9], but not in non-human primates [20]. Likewise, we did not observe any substantial bone uptake in our clinical [^{18}F]FDHT PET images either (unpublished data). In contrast to primates, rats do not have SHBG in their plasma. This plasma protein binds ^{18}F-labeled steroids like [^{18}F]FDHT and [^{18}F]FES and protects them from degradation. Because of the species differences in metabolic stability, it may still be warranted to investigate the feasibility of brain AR imaging in primates.

Since the accumulation of [^{18}F]fluoride in the cranial bones is located very close to the brain and the spatial resolution of the PET camera is limited (1.35 mm in the center of the field of view), the tracer uptake in peripheral rat brain areas is likely affected by spill-over of radioactivity from the bones into the brain. Indeed, the PET imaging data demonstrated that the tracer uptake (SUV) in brain regions close to the bones was generally higher than tracer uptake in centrally located brain regions. Moreover, PET indicated that tracer uptake in the brainstem was significantly higher in sham-orchiectomized rats, mimicking the differences observed in cranial bones. These observations were not found in the ex-vivo biodistribution results, suggesting that the effect were related to the imaging technique.

Kinetic modeling studies showed that kinetics in brain areas lying close to the cranial bones, such as amygdala, cerebellum, frontal cortex, occipital, temporal, parietal cortex and pituitary, could be better fitted with Patlak analysis, suggesting irreversible tracer kinetics. Likewise, tracer kinetics in the cranial bones could also be well described by Patlak graphical analysis. On the other hand, Logan analysis gave better fits for central brain regions like BNST, thalamus, striatum, hippocampus and hypothalamus, indicating that tracer uptake in these regions shows reversible kinetics. These results support the presence of a substantial spill-over effect from the irreversibly trapped radioactivity in the bones into the ROIs of the peripheral brain regions. Therefore, we eliminated the peripheral brain regions from the PET image analysis and pharmacokinetic modeling.

Kinetic modeling showed that the tracer uptake in the central brain regions could be well described by the 1TCM. In fact, model fits were more stable for the 1TCM than for 2TRCM and the 1TCM provided V_T values with less variability. Moreover, the BP_{ND} calculated with the 2TRCM also showed substantial variability between individual animal

within a single group, probably because of the low values for k_3 and k_4. A plausible explanation for the high variability in the results of the 2TRCM could be a low expression level of the target receptor in the brain. Consequently, only a small fraction of the tracer in the brain is receptor bound (second tissue compartment). These observations are supported by receptor binding studies that show that the number of high-affinity AR in the brain is substantially lower than in the ventral prostate [21,22].

Despite the higher expression of AR in the ventral prostate than in the brain, we could not detect any significant inhibition of [^{18}F]FDHT uptake in the prostate by androgens in sham-orchiectomized or DHT-treated rats. In contrast, Liu et al. [9] showed in an ex-vivo biodistribution study that [^{18}F]FDHT uptake in the prostate was approximately 70% reduced by co-injection of the tracer with testosterone, although no statistical analysis of this effect was provided. This apparent discrepancy between the results of the two studies can be explained by major differences in the experimental procedures, including differences in rat strain (Sprague Dawley vs. Wistar-Unilever), body weight (175 g vs. 350 g, reflecting age differences), anesthesia (ether vs. isofluran), time point of termination (2 h vs. 90 min p.i.) and blocker (0.2 mg/kg testosterone vs. 1 mg/kg DHT). However, probably the most important difference between the studies is the method of androgen deprivation (diethylstilbestrol for 24 h vs. orchiectomy for 15 days). Greenstein et al. [21] found that the androgen receptor expression in the ventral prostate – but not in the brain – strongly depends on the time after orchiectomy. After 0.75 days of androgen deprivation, AR density in the prostate was about 2.5-fold increased, whereas AR density was normalized again after 21 days. This suggests that the AR expression in the prostate was substantially higher in the animal model used by Liu and coworkers than in the animals in our study [9]. Another important difference between the studies, is the arterial blood sampling during the PET scan. In our study, 16 blood samples of approximately 0.1 - 0.2 ml were taken to construct a plasma input function for modeling. As a result, approximately 2 ml of blood, including a substantial amount of the injected radioactivity, was withdrawn from the rat. Because of some variation in the volume of the blood samples, the sampling protocol has probably led to an increase in the inter-individual variability in the tissue uptake of the tracer.

In this study, we also found that [^{18}F]FDHT uptake in the brain is not significantly affected by endogenous androgens, nor could administration of a 1 mg/kg dose of DHT significantly reduced tracer uptake. These results indicate that specific AR-mediated uptake could not be detected by [^{18}F]FDHT PET. Our results are in agreement with an AR binding study with [^{3}H]DHT [23]. This study also could not detect any significant differences in AR-mediated binding in the brain of castrated and non-castrated rats. Moreover, androgen treatment did not have any effect on AR binding in that study either.

Instead of AR specific binding, a tendency towards higher brain uptake in the sham-orchiectomized rats (and to a lesser extend in DHT-treated rats) was observed. A potential explanation for this tendency could be that the tonic levels of endogenous androgens in sham-orchiectomized rats and the short exposure to DHT in DHT-treated rats have increased the tracer delivery to the brain. This hypothesis is supported by the observation by Azad et al. [24] that cerebral perfusion is reduced in hypogonadal men. This effect on cerebral perfusion can be reverse by the administration of testosterone.

In situ hybridization studies on rat brain slices showed that AR expression varies between brain regions; it is highest in areas like amygdala, hippocampus, hypothalamus, BNST, brainstem and cerebellum [25]. In the current study, however, we could not find any correlation between [^{18}F]FDHT uptake (SUV, BP or V_T) and published expression levels of AR in the rat brain [25] (data not shown). In this context it should be noted that AR expression in the brain is often restricted to small regions like medial preoptic, arcurate, and ventromedial nuclei of the hypothalamus, the medial nucleus of the amygdala and the CA-1 hippocampus [26]. The spatial resolution of the small animal PET camera is not sufficient to accurately visualize these small areas and consequently any specific signal from these small regions would be averaged with the surrounding tissue in the same voxel, yielding a substantial partial volume effect. The low expression levels in the brain, the small areas in which the receptors are expressed and the extensive metabolism of the tracer in rats seem to be major contributors to the lack of specific binding found in this [^{18}F]FDHT PET study.

5. Conclusion

In this study, we evaluated [^{18}F]FDHT PET as a tool to quantify AR expression in the brain. Our results show that [^{18}F]FDHT is rapidly metabolized. Uptake of [^{18}F]FDHT in the rat brain is low and no specific binding to the AR could be detected. Taken together, these results indicate that [^{18}F]FDHT PET is not a suitable technique to monitor AR expression in the rat brain.

Acknowledgement

This project was partly funded by Jan Kornelis de Cock-Stichting foundation, Groningen, the Netherlands, with the project number 2013–39. No other potential conflict of interest with this article was reported

References

[1] Höfer P, Lanzenberger R, Kasper S. Testosterone in the brain: neuroimaging findings and the potential role for neuropsychopharmacology. Eur Neuropsychopharmacol 2013;23:79–88. http://dx.doi.org/10.1016/j.euroneuro.2012.04.013.
[2] Carré JM, McCormick CM, Hariri AR. The social neuroendocrinology of human aggression. Psychoneuroendocrinology 2011;36:935–44. http://dx.doi.org/10.1016/j.psyneuen.2011.02.001.
[3] Lehmann DJ, Hogervorst E, Warden DR, Smith AD, Butler HT, Ragoussis J. The androgen receptor CAG repeat and serum testosterone in the risk of Alzheimer's disease in men. J Neurol Neurosurg Psychiatry 2004;75:163–4.
[4] Irie F, Strozyk D, Peila R, Korf ES, Remaley AT, Masaki K, et al. Brain lesions on MRI and endogenous sex hormones in elderly men. Neurobiol Aging 2006;27:1137–44. http://dx.doi.org/10.1016/j.neurobiolaging.2005.05.015.
[5] Zitzmann M. Testosterone and the brain. Aging Male 2006;9:195–9. http://dx.doi.org/10.1080/13685530601040679.
[6] Seidman SN, Roose SP. The sexual effects of testosterone replacement in depressed men: randomized, placebo-controlled clinical trial. J Sex Marital Ther 2006;32:267–73. http://dx.doi.org/10.1080/00926230600575355.
[7] Cooke B, Hegstrom CD, Villeneuve LS, Breedlove SM. Sexual differentiation of the vertebrate brain: principles and mechanisms. Front Neuroendocrinol 1998;19:323–62. http://dx.doi.org/10.1006/frne.1998.0171.
[8] Khayum MA, Doorduin J, Glaudemans AWJM, Dierckx RAJO, de Vries EFJ. PET and SPECT imaging of steroid hormone receptors. In: Dierckx RAJO, Otte A, de Vries EFJ, van Waarde A, Luiten PGM, editors. PET and SPECT Neurobiological. Systems. Springer; 2014. p. 377–408.
[9] Liu A, Dence CS, Welch MJ, Katzenellenbogen JA. Fluorine-18-labeled androgens: radiochemical synthesis and tissue distribution studies on six fluorine-substituted androgens, potential imaging agents for prostatic cancer. J Nucl Med 1992;33:724–34.
[10] Zanzonico PB, Finn R, Pentlow KS, Erdi Y, Beattie B, Akhurst T, et al. PET-based radiation dosimetry in man of 18 F-fluorodihydrotestosterone, a new radiotracer for imaging prostate cancer. J Nucl Med 2004;45:1966–71.
[11] Dehdashti F, Picus J, Michalski JM, Dence CS, Siegel BA, Katzenellenbogen JA, et al. Positron tomographic assessment of androgen receptors in prostatic carcinoma. Eur J Nucl Med Mol Imaging 2005;32:344–50. http://dx.doi.org/10.1007/s00259-005-1764-5.
[12] Fedoruk MN, Giménez-Bonafé P, Guns ES, Mayer LD, Nelson CC. P-glycoprotein increases the efflux of the androgen dihydrotestosterone and reduces androgen responsive gene activity in prostate tumor cells. Prostate 2004;59:77–90. http://dx.doi.org/10.1002/pros.10354.
[13] Sar M, Stumpf WE. Distribution of androgen target cells in rat forebrain and pituitary after [3H]-dihydrotestosterone administration. J Steroid Biochem 1977;8:1131–5.
[14] Banks WA, Morley JE, Niehoff ML, Mattern C. Delivery of testosterone to the brain by intranasal administration: comparison to intravenous testosterone. J Drug Target 2009;17:91–7. http://dx.doi.org/10.1080/10611860802382777.
[15] Beattie BJ, Smith-Jones PM, Jhanwar YS, Schöder H, Schmidtlein CR, Morris MJ, et al. Pharmacokinetic assessment of the uptake of 16beta-18 F-fluoro-5alpha-dihydrotestosterone (FDHT) in prostate tumors as measured by PET. J Nucl Med 2010;51:183–92. http://dx.doi.org/10.2967/jnumed.109.066159.
[16] Corvol P, Bardin CW. Species distribution of testosterone-binding globulin. Biol Reprod 1973;8:277–82.
[17] Rasmussen MK, Brunius C, Ekstrand B, Zamaratskaia G. Expression of hepatic 3β-hydroxysteroid dehydrogenase and sulfotransferase 2A1 in entire and castrated male pigs. Mol Biol Rep 2012;39:7927–32. http://dx.doi.org/10.1007/s11033-012-1637-5.
[18] Chen G, Bourneuf E, Marklund S, Zamaratskaia G, Madej A, Lundström K. Gene expression of 3beta-hydroxysteroid dehydrogenase and 17beta-hydroxysteroid

dehydrogenase in relation to androstenone, testosterone, and estrone sulphate in gonadally intact male and castrated pigs. J Anim Sci 2007;85:2457–63. http://dx.doi.org/10.2527/jas. 2007-0087.
[19] Pirog EC, Collins DC. Metabolism of dihydrotestosterone in human liver: importance of 3alpha- and 3beta-hydroxysteroid dehydrogenase. J Clin Endocrinol Metab 1999; 84:3217–21. http://dx.doi.org/10.1210/jcem.84.9.5963.
[20] Bonasera TA, O'Neil JP, Xu M, Dobkin JA, Cutler PD, Lich LL, et al. Preclinical evaluation of fluorine-18-labeled androgen receptor ligands in baboons. J Nucl Med 1996;37:1009–15.
[21] Greenstein BD. Androgen receptors in the rat brain, anterior pituitary gland and ventral prostate gland: effects of orchidectomy and ageing. J Endocrinol 1979;81:75–81.
[22] Greenstein BD. Analysis of activated androgen receptors in rat brain and anterior pituitary and ventral prostate glands: nuclear binding and RNA polymerase activity. J Endocrinol 1984;102:181–8.
[23] Handa RJ, Kerr JE, DonCarlos LL, McGivern RF, Hejna G. Hormonal regulation of androgen receptor messenger RNA in the medial preoptic area of the male rat. Brain Res Mol Brain Res 1996;39:57–67.
[24] Azad N, Pitale S, Barnes WE, Friedman N. Testosterone treatment enhances regional brain perfusion in hypogonadal men. J Clin Endocrinol Metab 2003;88:3064–8. http://dx.doi.org/10.1210/jc.2002-020632.
[25] Simerly RB, Chang C, Muramatsu M, Swanson LW. Distribution of androgen and estrogen receptor mRNA-containing cells in the rat brain: an in situ hybridization study. J Comp Neurol 1990;294:76–95. http://dx.doi.org/10.1002/cne.902940107.
[26] Sar M, Lubahn DB, French FS, Wilson EM. Immunohistochemical localization of the androgen receptor in rat and human tissues. Endocrinology 1990;127:3180–6. http://dx.doi.org/10.1210/endo-127-6-3180.